Morphometric identification of human molars using machine learning

Wataru Morita[1]* and Naoki Morimoto[2]

[1] Department of Anthropology, National Museum of Nature and Science,
4–1–1 Amakubo, Tsukuba City, Ibaraki 305–0005, Japan
[2] Laboratory of Physical Anthropology, Department of Zoology, Graduate School of Science,
Kyoto University, Kitashirakawa Oiwakecho, Sakyo, Kyoto City, Kyoto 606–8502, Japan
*E-mail address: wmorita@kahaku.go.jp
*corresponding author.
Address: 4–1–1 Amakubo, Tsukuba City, Ibaraki 305–0005, Japan
Phone: ＋81–(0)29–853–8184
FAX: ＋81–(0)29–853–8998

Abstract　Identifying individual tooth (tooth class and type within it) is a fundamental skill for anthropologists. It is always required for basic description in the fieldwork. Besides, it is vital to identify dental specimens in the studies to infer phylogenetic relationships and species classification. Likewise, the identification of teeth is highly relevant in the primary education of dentistry. However, the characteristics described in standard textbooks do not necessarily apply to all teeth due to broad inter-individual variation of morphology. While the qualitative description of dental traits is useful, it better be constructed on the ground of quantitative analysis. Here, we introduced a method that combines the technique of geometric morphometrics and machine learning. Specifically, we used the method of morphometric mapping to quantify and visualize three-dimensional tooth crown morphology of human upper molars and to extract multiple morphological parameters which can then be submitted to machine learning. Results show that the classification accuracy is maximized when using the x component of vertex normal toward mesio-distal direction with a small filter size for noise reduction. The mesio-distal gradient of tooth crown morphology is highly relevant for molar type identification with algorithmic processing, which is underpinned by the morphogenetic process of tooth formation.
KeyWords: Morphometric mapping, Artificial intelligence, Data mining, EDJ

Introduction

Most mammals, including modern humans, generally have three molar teeth. The pattern of inter-molar variation, that is, metameric variation of molars, varies among species. To explain metameric variation systematically, the inhibitory cascade model (ICM) was proposed (Kavanagh *et al.*, 2007). The relationship of relative molar size between M1, M2, and M3 (first, second, and third molars) was formulated from experimental data of murine rodents and correlated with dietary habits (Polly, 2007). Although

it has been pointed out that this model does not always adequately describe metameric variation in some mammalian clades (Bernal *et al.*, 2013; Roseman and Delezene, 2019) and other indices such as the molar module component (MMC) have been proposed (Hlusko *et al.*, 2016), the relationship between molar size and shape provides relevant information on dentition formation during development. In actual, the ICM is also widely used to explore dietary adaptation and phylogenetic relationships in primates (Bermúdez De Castro *et al.*, 2021; Carter and Worthington, 2016; Schroer and Wood, 2015). In the evolution of the human lineage, Evans *et al.* (2016) revealed that there is a difference in reversal

position of dental reduction between australopiths and genus *Homo*, indicating that intermolar variation has been evolutionarily changed in the human lineage.

The identification of individual tooth is a fundamental skill for all researchers whose work involves dentition. In particular, it is vital to identify dental specimens (tooth class and type within it) in the studies of evolutionary biology to infer phylogenetic relationships and the classification of species. Similarly, the identification of teeth is highly relevant to the primary education of dentistry (Bailey and Hublin, 2007; Hillson, 1996, 2005; Nelson and Wheeler, 2015). The characteristics described in standard textbooks, however, do not necessarily apply to all teeth due to considerable inter-individual variation of morphology. Although the qualitative description of dental traits is practical and meaningful, it should be corroborated quantitatively.

In this study, we use the morphometric mapping method, which can quantitatively evaluate the 3D morphology (Morita *et al.*, 2016a). The morphometric mapping method unfolds a 3D surface model into a 2D image (morphometric "map") using several morphometric variables. Tooth identification using the morphometric mapping method also contributes to a conceptual appreciation of tooth characteristics and essential points for identification. The morphological parameters used in morphological mapping, such as sharpness, the direction of the surface, and relative height, may help us understand which morphological features we should focus on for classification.

Since the 2000s, the rise of artificial intelligence, including machine learning and deep learning, has accelerated automated pattern recognition and classification (Ahmed *et al.*, 2019; Emmert-Streib *et al.*, 2020; Gezawa *et al.*, 2020; Ray, 2019). Such human-free algorithms provide us with objective classification of 3D shapes and make us recognize crucial characters for tooth identification in a reflective manner (Monson *et al.*, 2018). Combined with morphometrics, there are some attempts to optimize parameters by machine learning for the purpose of variable selection (Morita *et al.*, 2020a; Plyusnin *et al.*, 2008). In this study, we combine morphometric mapping with artificial intelligence to classify human maxillary molars.

Materials and Methods

The materials consist of 176 human upper molars (Table 1). Sex was undetermined for most of the sample, which was a mixture of populations from different periods and regions (from Neolithic, medieval, early modern, and modern populations in the Japanese archipelago). Teeth that had completed crown formation and maintained unworn enamel–dentine junction (EDJ) were used. The EDJ was used to elude the effects of dental attrition on parameterization and classification of molar teeth. A tooth crown consists of two tissue layers: enamel and dentine, whose boundary can be observed as EDJ. Due to the high correlation between EDJ and the shape of the outer enamel surface of teeth, EDJ has been extensively studied in dental anthropology (Blinkhorn *et al.*, 2021; Morita *et al.*, 2014; Skinner *et al.*, 2009). Volume reconstructions of human molars were constructed from various μCT scans acquired with the following scanners: the ScanXmateA080S, Comscantecno, Japan (housed at Kyoto University, and scans made at voxel resolutions of 31–32 μm); the ELE SCAN, Nittetsu Elex, Japan (housed at Niigata University, and scans made at voxel resolutions of 30 μm). The CT image stacks were filtered with a median filter to facilitate tissue segmentation, and triangular mesh models of the 3D EDJ surface were reconstructed using the software Amira 4.1 (Mercury Systems). We analyzed both right and left teeth to maximize sample size. Eventu-

Table 1.　Sample structure

Molar type	N
UM1	62
UM2	54
UM3	60
Total	176

ally, all specimens were considered as left by mirroring the teeth from the right side.

Prior to the morphometric analyses, each of the EDJ surface models was aligned as follows. First, the intercuspal ridges among the four main cusp tips (para-cone, protocone, metacone, and hypocone) of each tooth were manually digitized on the surface model, and the least-squares plane of the occlusal fovea was computed. In specimens with an undeveloped or absent hypocone (i.e. most of UM3s), the distolingual edge of the occlusal fovea was traced. Each molar specimen was then positioned with the least-squares plane of the occlusal fovea in parallel with the xy-plane of the Cartesian coordinate system and centered using the centroid of the occlusal fovea. Second, we digitized landmarks along the cervical line to calculate the centroid of the cervix. We then defined a plane parallel to the occlusal plane containing the centroid of the cervical line as the cervical plane. The molar was placed so that the cervical plane was paralleled to xy-plane. Each molar was centered on matching with the centroid of this Cartesian coordinate system, followed by shifting-down of the 3D model along z-axis up to upper 80% of an entire tooth crown (from the highest point to the cervical plane) being above xy-plane.

To parameterize three-dimensional EDJ, each surface model was sectioned by 300 vertical planes radiating from the z-axis, perpendicular to the occlusal fovea (L = 300). Each vertical cross-section had 300 points sampled along the outline of the EDJ surface, running from the z-axis to the endpoint at $z = 0$ (K = 300). For these equidistant 300 sampled points along the 300 equiangular sections, the following morphometric parameters were recorded: surface curvature (c), height from the cervical plane (h), horizontal distance from the centroid, i.e., radius (r), and vertex normal which represents the direction of the local area in 3D as a unit vector (Nxyz). The data sets of each molar consist of K × L matrices of each four parameters of six variables (c, h, r, and Nxyz). Note that the surface curvature c is calculated three-dimensionally but sampled along the cross-

sections.

These morphometric variables were mapped on a polar coordinate system (d, θ), where d denotes the standardized position along each cross-sectional outline ($d = 0 \rightarrow 1$: centroid$\rightarrow$ cervix), and θ denotes the anatomical direction ($\theta = 0° \rightarrow 360°$: buccal$\rightarrow$mesial$\rightarrow$lingual$\rightarrow$distal $\rightarrow$buccal). The EDJ morphology could thus be visualized as 2D image M (d, θ). Those morphometric maps are shown as false-color maps. Each component of vertex normal vector (Nx, Ny, Nz) is assigned to three sets of an RGB color value, respectively, and represented as a single map. For facilitating visual inspection, morphometric maps are reconstructed to represent an outline of the tooth crown by padding the background depending on relative length at the cervix. The scaling effects on the variables c, h, and r were normalized by centroid size (CS, the square root of the summed squared distances calculated from height and radius). This approach is analogous to standardization by centroid size in geometric morphometrics (Bookstein, 1991). Each row of the K × L matrix for each specimen was sequentially weighted by a concentrically subdivided area with radius one and constant internal angle (= 1/L) that was equidistantly sectioned (= 1/K). Each specimen was preoriented according to the anatomical axis. Then, 2D-Fourier transforms F(Mi) of all Mi (i = 1, 2, …, n) were calculated (M had natural periodicity in θ). These K × L sets of Fourier coefficients of each specimen's 3D EDJ surface model are represented as a point in the multidimensional Fourier space. The optimal fitting for all the maps around the z-axis was achieved by iteratively minimizing inter-specimen distance in Fourier space through rotation around θ. After all the specimens were aligned by best-fit, we carried out machine learning to select the combination of morphometric parameters and the number of set of Fourier coefficients (i.e., the size of low-pass filtering for noise reduction in Fourier space) to reduce the number of variables relative to the number of specimens and to achieve molar type identification.

Machine learning was performed to maximize

the classification accuracy of three types of human upper molars (UM1, UM2, and UM3). We executed multiclass error-correcting output codes (ECOC) model (Fürnkranz, 2002), using five types of leaners: decision tree, linear classification, discriminant analysis, support vector machine (SVM), and k-nearest neighbors (number of neighbors was set to 1, 3, and 5 with neighborhood defined by Euclidean distance). The 10-fold cross-validation was performed as a measure of model accuracy with a total of seven classification models described above. We compared 12 combinations of morphometric variables by adjusting the size of low-pass filtering from 1 to 50: c, h, r, Nx, Ny, Nz, chr, hr, chrNxyz, Nxyz, Nxy, Nxyzr.

After the data mining procedure using machine learning, we conducted between-group principal components analysis (bgPCA). Morphometric maps were reconstructed by transforming an arbitrary point along the bgPC axis into its corresponding sets of Fourier coefficients for use in reconstructing morphometric maps by an inverse Fourier transformation. All calculations were performed in MATLAB 9.10 (Math-Works, USA).

Results

We applied variable selection algorithms by utilizing machine learning to pick up the combination of morphometric parameters and the size of low-pass filtering to optimize the classification of three types of human upper molars. To explore a relatively broad range of morphological properties, we compared twelve types of map combina-
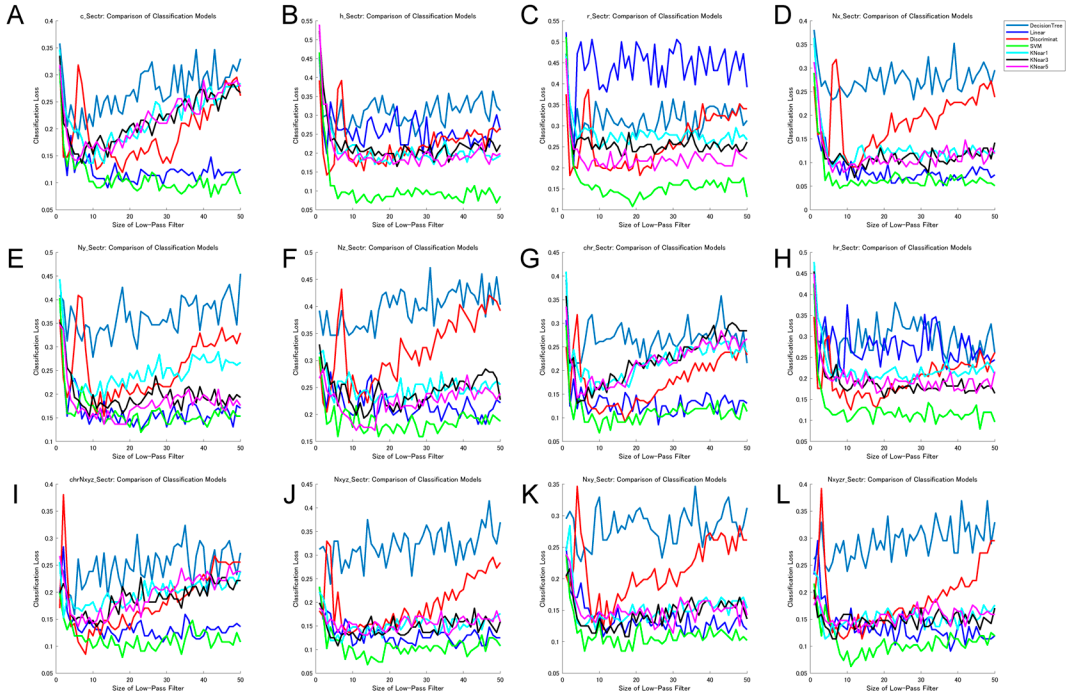
Fig. 1.   Results of machine learning of seven types of probabilistic classification models for 12 map variable combinations. (A) c: surface curvature; (B) h: height; (C) r: radius; (D) Nx: x component of vertex normal; (E) Ny: y component of vertex normal; (F) Nz: z component of vertex normal; (G) chr: surface curvature, height, and radius; (H) hr: height and radius; (I) chrNxyz: surface curavutre, height, radius, and vertex normal; (J) Nxyz: vertex normal; (K) Nxy: two elements of vertex normal; (L) Nxyzr: vertex normal and radius. Size of low-pass filter is equal to the number of sets of Fourier coefficients for the analysis. SVM, support vector machine. KNear, k-nearest neighbor (number of neighbors was set to 1, 3, and 5).

Table 2. Top twenty probabilistic classification models in machine learning for human upper molars

Rank	Size of low-pass filter	Classification loss	Combination of maps	Learner
1	8	0.045454545	Nx	SVM
2	36	0.051136364	Nx	Linear
3	6	0.051136364	Nx	SVM
4	9	0.051136364	Nx	SVM
5	10	0.051136364	Nx	SVM
6	13	0.051136364	Nx	SVM
7	15	0.051136364	Nx	SVM
8	30	0.051136364	Nx	SVM
9	31	0.051136364	Nx	SVM
10	34	0.051136364	Nx	SVM
11	37	0.051136364	Nx	SVM
12	42	0.051136364	Nx	SVM
13	50	0.051136364	Nx	SVM
14	22	0.056818182	Nx	Linear
15	23	0.056818182	Nx	Linear
16	12	0.056818182	Nx	SVM
17	17	0.056818182	Nx	SVM
18	18	0.056818182	Nx	SVM
19	21	0.056818182	Nx	SVM
20	25	0.056818182	Nx	SVM

Nx, x component of vertex normal. SVM, Support vector machine; Linear, Linear classification.

tions by adjusting the size of low-pass filtering in seven different classification models (five basic learners: decision tree, linear, discriminant, support vector machine, and k-nearest neighbor). The cross-validation was executed to calculate the classification accuracy of each model with mean classification loss, where data was randomly partitioned into ten subsets, and one subset was used to validate the model trained using the remaining subsets. Support vector machine (SVM) was consistently a better classifier for human molar identification (Fig. 1). On the contrary, decision tree and discriminant analysis get worse as the filter size gets larger. K-nearest neighbor models (K = 1, 3, and 5) demonstrated a similar tendency of classification loss in different data sets. Linear classification, as with SVM, results in low classification loss stably in most cases except for r-M, which may be dependent on the data structure. The top 20 models deriving from 600 data sets (12 combinations of morphometric variables by 50 sizes of low-pass filtering; SI Tables 1–12) are shown in Table 2. The morphometric parameter of these top 20 models was the x component of vertex normal, whose accuracies (accuracy = 1–averaging cross-validation classification loss) are about 95%. Among them, between-group principal component analysis (bgPCA) was performed using the best set of variables (x component of vertex normal with filter size equal to eight) to visualize shape variation.

Fig. 2 shows UM shape variation in a bgPC space and corresponding patterns of shape variation along bgPC1 and bgPC2, which comprise 91.0% and 9.0% of the total variation, respectively. Although morphometric parameters used for multivariate analysis differ, the resulting plot is largely consistent with Morita *et al.* (2016a).

Along PC1, there is a continuous transition from UM1, UM2, and UM3. Interpretation of the shape change in Nx-M is a delicate matter, but bgPC1 captures the complexity of the occlusal surface. Slopes within an occlusal table are well-separated, especially distal triangular fovea by an oblique ridge in higher bgPC1, whereas lower PC1 has a simple occlusal fovea. The bgPC2 separates UM2 from UM1 and UM3. Shape variation of bgPC2 is associated with the relative expansion along the buccolingual axis, where higher bgPC2 shows a relatively larger buccal area; on the other hand, dental structures are equally distributed in lower bgPC2.

The distribution of adjacent molar types (i.e., UM1–UM2 and UM2–UM3) are overlapped in morphospace. In Fig. 2B, the 3D surface models and corresponding Nx-Ms demonstrate shape variation within the molar type with both the typical morphology of each tooth type located almost at the center of the variation of each molar type and the atypical specimen located in the region of adjacent molar types. Each of these outliers has a morphology that more closely resembles the typical shape of the adjacent tooth type than the typical shape of the tooth type to which it originally belongs.

Fig. 3 visualizes the metameric variation of human upper molars using several morphometric parameters. Since the metameric shape change
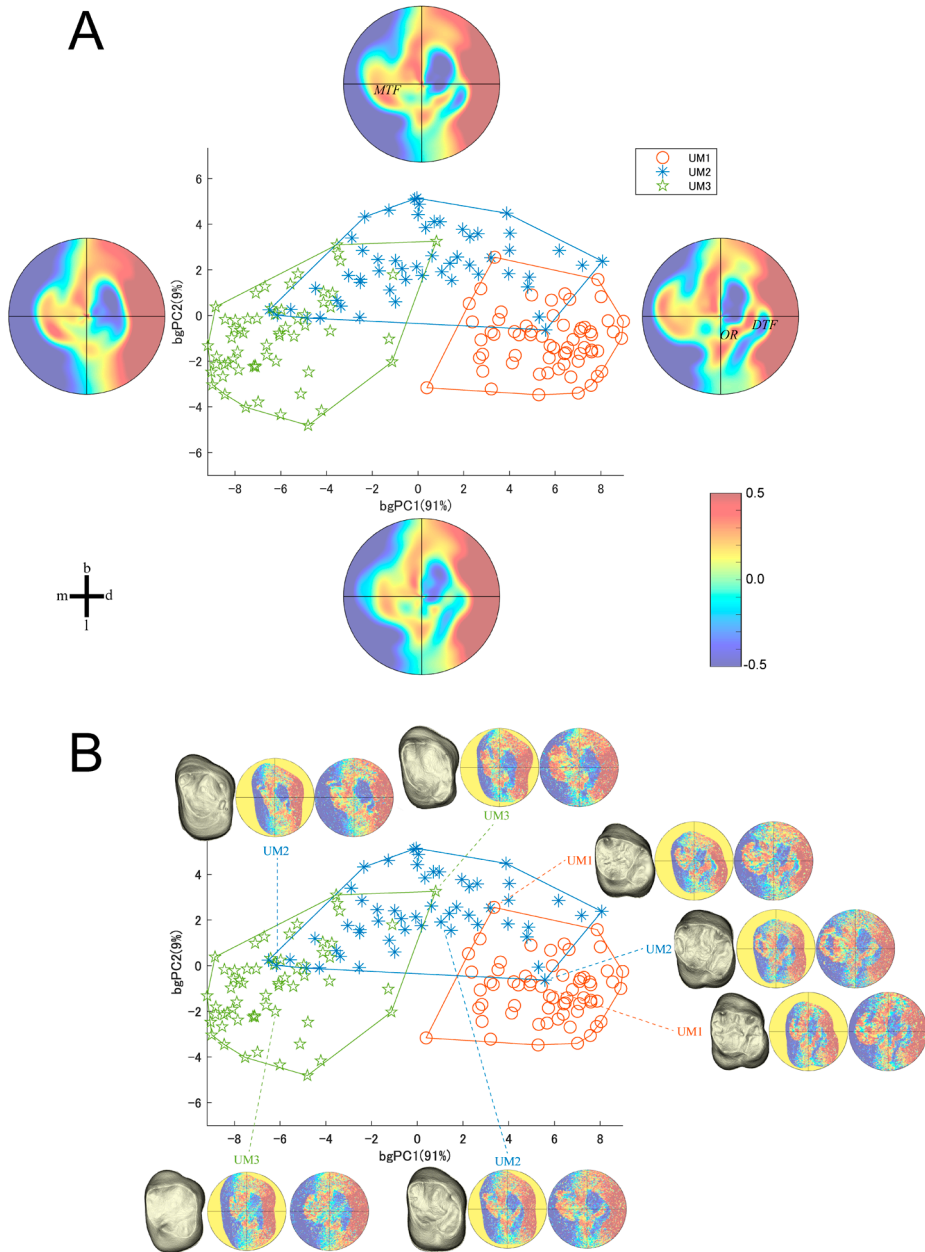
Fig. 2.　Metameric variation in human UMs. (A) Molar shape variation in between-group (bg) PC space (along bgPC1 and bgPC2) using the best classifier [x component of vertex normal (Nx) with first eight sets of Fourier coefficients]. Symbols used in the bgPC graph: red open circles: UM1, blue asterisks: UM2, green open stars: UM3. Major patterns of variation are represented by morphometric maps (Nx-M, FT 8) visualising ± 1 s.d. along each bgPC axis: bgPC1: (−) round and simple occlusal surface/ (+) mesiodistally elongated and highly patched relief of occlusal surface. bgPC2: (−) enlarged buccal area in occlusal surface/ (+) compact crown structure. (B) Shape variation depicted on bgPC1 and bgPC2. 3D model and corresponding x component of vertex normal map (left: outlined at cervix, right: circular representation) of pointed specimens are provided to demonstrate shape variation. MTF: mesial triangular fovea, DTF: distal triangular fovea, OR: oblique ridge. b: buccal, m: mesial, l: lingual, d: distal.
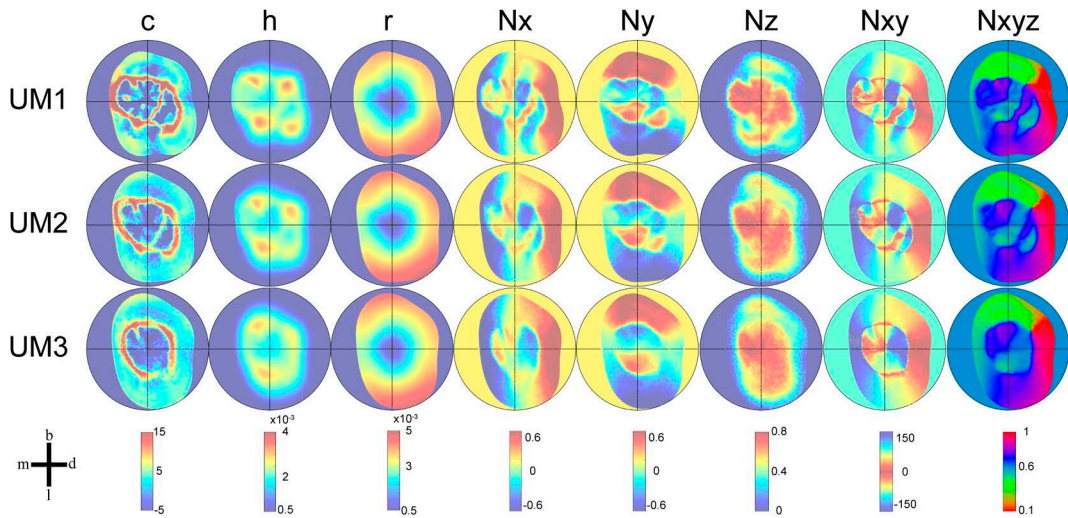
Fig. 3. Average morphometric maps (six univariate morphometric parameters and two combinations of vertex normal) of UM1, UM2 and UM3 (from top to bottom) in humans. All maps are outlined at the cervix. b: buccal, m: mesial, l: lingual, d: distal.

largely runs parallel to the bgPC1 axis, morphological transition proceeds with gradual simplification of occlusal features from mesial to distal. The most notable shape change is hypocone reduction.

Discussion

We examined the accuracy of identification in human upper molars using six univariate maps consisting of surface curvature, height, radius, and each of three components of the normal vector, plus six combinations of several variables among them (Fig. 1). For most morphometric parameters, the combination with others does not stunningly increase the classification accuracy. However, in the case of r-M, the classification loss was decreased by combining with other maps, which would rather stem from the offset by the contribution of other parameters. Thus, a simple increase in the amount of information does not necessarily have a positive effect on molar type identification, nor does it mean that there is a correlation between them. Similarly, a larger filter size in low-pass filtering does not necessarily make the classification accuracy better. Instead, it could increase classification loss

depending on the learner used in the algorithm of machine learning. Considering the possibility that noise may be included as the filter size increases, as for the filter size in the low-pass filtering process, it seems appropriate to set a value between 10 and 20 as the size of low-pass filtering to identify molar types. In this study, machine learning was used for the identification of tooth types. However, the application of artificial intelligence, such as image classification technology based on deep learning, can also be widely applicable to fossil classification and/or phylogenetic estimation (Yi *et al.*, 2021).

We used only the x component of vertex normal (Nx) which gave the best scores in classification accuracy to represent molar shape variation in morphospace, and they were different from those in Morita *et al.* (2016b), where a set of variables consisting of surface curvature, height, and radius was exploited. Nevertheless, the topology of molar type distribution in bgPC space is almost the same, making the results more robust. Furthermore, the bgPC1 captures a gradual shape change from UM1 to UM3, which is related to the shape change from a complex configuration to a simple one in the occlusal table. This major tendency of metameric varia-

tion is also shared across hominoids (Morita *et al.*, 2020b). Along the bgPC2 axis, UM2, which shows markedly reduced hypocone relative to the other earlier-forming three cusps, is distinguished from UM1 in having hypocone of sufficient size and UM3 whose cusps are degraded on the whole. This prominent hypocone reduction is unique to humans (Morita *et al.*, 2020b). Since these shape changes have also been confirmed as valuable features for differentiating human molar types, it may be beneficial for students in dentistry to learn how to identify teeth by taking the similarities and differences between the teeth of hominoids, such as chimpanzees, gorillas, and orangutans into consideration.

It is also worth noting that Nx is the most useful for molar identification. The accuracy of classification by machine learning was shown to be close to at most 95% (Table 2). The *x*-axis in the present coordinate system corresponds to the anatomical mesiodistal axis and is thought to sensitively project shape changes in the crown structure along the mesiodistal axis. In conventional dental metric analyses, it is impossible to extract and analyze the single morphometric parameter that reflects the mesiodistal axis. Unlike other geometric morphometric methods, most of which use coordinates for analysis, the morphometric mapping method has obvious merit that morphological attributes derived from the object can be decomposed into several morphometric parameters to quantify and visualize three-dimensional shapes.

Thus, the mesio-distal gradient between molars was proven to be essential for molar type identification in terms of algorithmic processing. While, this mesio-distal gradient among dentition has been explained by the patterning cascade model as the difference between cusps in a single crown (Jernvall and Jung, 2000) and by the inhibitory cascade model as the difference between molars (Kavanagh *et al.*, 2007). In both models, the same unit is repeatedly formed from mesial to distal by the interaction between activator and inhibitor, and morphological reduction could occur at the distal part due to a gradual

decline of patterning potency. When it comes to morphological comparison between human molar types, it is often pointed out that UM1 has a stable and fixed morphology. At the same time, UM3 shows more considerable shape variation and is more atypical. The perspective underpinned by the developmental models that UM1 exhibits a more negligible difference in morphological complexity within the tooth crown while UM3 has a larger gradation from mesial to distal in crown structure is also important as a criterion for the identification of human molars.

Overall, it appears machine learning is a powerful tool that can accurately identify tooth types based on various morphometric variables and infer an underlying developmental pattern. Combining artificial intelligence with morphometric mapping showed a potential of automated variable selection for precise tooth identification and should be applicable to detect characteristics in developmental process or test evolutionary hypotheses and taxonomic discrimination of fossils for future studies (Monson *et al.*, 2018; Yi *et al.*, 2021).

References

Ahmed, E., Saint, A., Abd, Cherenkova, K., Das, R., Gusev, G., Aouada, D., Ottersten, B., 2019. A survey on Deep Learning Advances on Different 3D Data Representations. *arXiv pre-print server*.

Bailey, S.E., Hublin, J.-J., 2007. Dental perspectives on human evolution: state of the art research in dental paleoanthropology. Springer.

Bermúdez De Castro, J.M., Modesto-Mata, M., Martín-Francés, L., García-Campos, C., Martínez De Pinillos, M., Martinón-Torres, M., 2021. Testing the inhibitory cascade model in the Middle Pleistocene Sima de los Huesos (Sierra de Atapuerca, Spain) hominin sample. *Journal of Anatomy*, 238, 173–184.

Bernal, V., Gonzalez, P.N., Perez, S.I., 2013. Developmental Processes, Evolvability, and Dental Diversification of New World Monkeys. *Evolutionary Biology*, 40, 532–541.

Blinkhorn, J., Zanolli, C., Compton, T., Groucutt, H.S., Scerri, E.M.L., Crété, L., Stringer, C., Petraglia, M.D., Blockley, S., 2021. Nubian Levallois technology associated with southernmost Neanderthals. *Scientific Reports*, 11.

Bookstein, F.L., 1991. Morphometric Tools for Landmark Data: Geometry and Biology. Cambridge University Press, Cambridge.

Carter, K.E., Worthington, S., 2016. The evolution of anthropoid molar proportions. *BMC Evolutionary Biology*, 16, 110.

Emmert-Streib, F., Yang, Z., Feng, H., Tripathi, S., Dehmer, M., 2020. An Introductory Review of Deep Learning for Prediction Models With Big Data. *Frontiers in Artificial Intelligence*, 3.

Evans, A.R., Daly, E.S., Catlett, K.K., Paul, K.S., King, S.J., Skinner, M.M., Nesse, H.P., Hublin, J.-J., Townsend, G.C., Schwartz, G.T., Jernvall, J., 2016. A simple rule governs the evolution and development of hominin tooth size. *Nature*, 530, 477–480.

Fürnkranz, 2002. Round robin classification. *Journal of Machine Learning Research*, 2.

Gezawa, A.S., Zhang, Y., Wang, Q., Yunqi, L., 2020. A Review on Deep Learning Approaches for 3D Data Representations in Retrieval and Classifications. *IEEE Access*, 8, 57566–57593.

Hillson, S., 1996. Dental anthropology. Cambridge University Press.

Hillson, S., 2005. Teeth, 2 ed. Cambridge University Press, Cambridge.

Hlusko, L.J., Schmitt, C.A., Monson, T.A., Brasil, M.F., Mahaney, M.C., 2016. The integration of quantitative genetics, paleontology, and neontology reveals genetic underpinnings of primate dental evolution. *Proceedings of the National Academy of Sciences of the United States of America*, 113, 9262–9267.

Jernvall, J., Jung, H.-S., 2000. Genotype, phenotype, and developmental biology of molar tooth characters. *American Journal of Physical Anthropology*, 113, 171–190.

Kavanagh, K.D., Evans, A.R., Jernvall, J., 2007. Predicting evolutionary patterns of mammalian teeth from development. *Nature*, 449, 427–432.

Monson, T.A., Armitage, D.W., Hlusko, L.J., 2018. Using machine learning to classify extant apes and interpret the dental morphology of the chimpanzee-human last common ancestor. *PaleoBios*, 35.

Morita, W., Morimoto, N., Jernvall, J., 2020a. Mapping molar shapes on signaling pathways. *PLoS Computational Biology*, 16, e1008436.

Morita, W., Morimoto, N., Kono, R.T., Suwa, G., 2020b. Metameric variation of upper molars in hominoids and its implications for the diversification of molar morphogenesis. *Journal of Human Evolution*, 138, 102706.

Morita, W., Morimoto, N., Ohshima, H., 2016a. Exploring metameric variation in human molars: a morphological study using morphometric mapping. *Journal of Anatomy*, 229, 343–355.

Morita, W., Morimoto, N., Ohshima, H., 2016b. Exploring metameric variation in human molars: a morphological study using morphometric mapping. *Journal of Anatomy*, 229, 343–355.

Morita, W., Yano, W., Nagaoka, T., Abe, M., Ohshima, H., Nakatsukasa, M., 2014. Patterns of morphological variation in enamel-dentin junction and outer enamel surface of human molars. *J Anat*, 224, 669–680.

Nelson, S.J., Wheeler, R.C., 2015. Wheeler's dental anatomy, physiology, and occlusion, 10th ed. Elsevier, Saunders.

Plyusnin, I., Evans, A.R., Karme, A., Gionis, A., Jernvall, J., 2008. Automated 3D phenotype analysis using data mining. *PLoS One*, 3, e1742.

Polly, P.D., 2007. Evolutionary biology: Development with a bite. *Nature* 449, 413–415.

Ray, S., 2019. A Quick Review of Machine Learning Algorithms. IEEE.

Roseman, C.C., Delezene, L.K., 2019. The inhibitory cascade model is not a good predictor of molar size covariation. *Evolutionary Biology*, 46, 229–238.

Schroer, K., Wood, B., 2015. Modeling the dental development of fossil hominins through the inhibitory cascade. *Journal of Anatomy*, 226, 150–162.

Skinner, M.M., Wood, B.A., Hublin, J.J., 2009. Protostylid expression at the enamel-dentine junction and enamel surface of mandibular molars of Paranthropus robustus and Australopithecus africanus. *J Hum Evol*, 56, 76–85.

Yi, Z., Zanolli, C., Liao, W., Wang, W., 2021. A deep — learning — based workflow to assess taxonomic affinity of hominid teeth with a test on discriminating *Pongo* and *Homo* upper molars. *American Journal of Physical Anthropology*.